Blended wing body configuration for hydrogen-powered aviation

Eytan J. Adler* and Joaquim R. R. A. Martins†
Department of Aerospace Engineering, University of Michigan, Ann Arbor, Michigan, 48109

Hydrogen aircraft have the potential to achieve greater climate impact reductions at a lower cost than aircraft powered by biofuels or other drop-in sustainable aviation fuels. But even as a liquid, hydrogen requires four times more volume than kerosene to store the same energy. Companies and researchers have suggested that the blended wing body configuration is well-suited to hydrogen because it can efficiently store the large fuel tanks. However, nobody has quantified this claim, at least publicly. We address this gap by comparing optimized kerosene and hydrogen versions of blended wing body and tube and wing aircraft. We find that the blended wing body configuration has only a small advantage for onboard hydrogen storage compared to a conventional tube and wing aircraft. Our models predict that with ambitious hydrogen tank technology assumptions, a hydrogen blended wing body uses 3.1% more energy than a kerosene blended wing body, while the energy increase for a tube and wing is 5.1%. An advantage of the blended wing body is that the energy consumption increase when adapting from kerosene to hydrogen fuel appears to be far less sensitive than the tube and wing's to empty weight and drag changes. Because we only compare hydrogen and kerosene usage within the same configuration, a hydrogen blended wing body may still consume substantially less energy than a hydrogen tube and wing. However, these results do call into question the assumed tank storage benefit of a hydrogen-powered blended wing body aircraft.

Nomenclature

A_{flapped}	fraction of wing area with flaps
BWB	blended wing body
b_{slat}	slat span to wing span ratio
C_D	drag coefficient
C_d	2D airfoil drag coefficient
C_f	skin friction coefficient
C_L	lift coefficient
C_l	2D airfoil lift coefficient
c_{flap}	flap chord to wing chord ratio
c_{slat}	slat chord to wing chord ratio
E	Young's modulus
f_{stiff}	multiplier to account for stiffeners
L	length
LH_2	liquid hydrogen
MAC	mean aerodynamic chord
MEOP	maximum expected operating pressure
MTOW	maximum takeoff weight
OEW	operating empty weight
P	pressure
Re	Reynolds number
r	radius
T&W	tube and wing
TSEC	thrust-specific energy consumption
TSFC	thrust-specific fuel consumption
t	thickness
t/c	airfoil thickness-to-chord ratio
W_{fuel}	fuel weight
$W_{\text{mission fuel}}$	mission fuel weight (excluding reserve)
W_{payload}	payload weight
W_{tank}	hydrogen tank weight
$W_{\text{total fuel}}$	fuel weight including reserve fuel
β	fraction of boundary layer that is laminar
δ	flap deflection angle
γ	safety factor
Λ	quarter chord sweep angle
η_{grav}	tank gravimetric efficiency
ρ	density
σ_{yield}	yield stress

I. Introduction

Climate change is driving renewed interest in hydrogen-powered aircraft because they emit no carbon dioxide in flight. These aircraft can decrease the CO_2 equivalent emissions by 50–99% [1, 2] compared to kerosene-powered

*Ph.D. Candidate, AIAA Member
†Pauline M. Sherman Collegiate Professor, AIAA Fellow

aircraft. Governments, particularly in Europe, have been motivated by climate change to regulate the commercial aviation industry and fund international programs to investigate the merits of hydrogen-powered aircraft. With the prospect of having to meet stricter regulations, large aerospace companies including Airbus [3], CFM International [4], Pratt & Whitney [5], and Rolls-Royce [6] have announced hydrogen projects.

Hydrogen as a gas at ambient temperature and pressure has far too low a density to fit on an aircraft—its storage would require hundreds of times the volume of the aircraft [7]. To store the necessary energy in a reasonable volume, the hydrogen must be liquefied by cooling it to 20 K. The low temperatures necessitate tanks with a low surface area-to-volume ratio to reduce the amount of heat entering the cryogenic fuel. These tanks can no longer be stored in the thin wingbox, as kerosene fuel is today. A common solution for tube and wing (T&W) configurations is to store the hydrogen in fuselage tanks [3, 8–12]. Figure 1a shows a popular fuselage packaging solution that allows the tanks to be as close to a sphere as possible because they use the full fuselage radius. However, this solution still increases the aircraft's weight and drag.

In recent decades, blended wing body (BWB) designs have matured [13]. Fuel burn reduction estimates range from 15 to 50% compared to T&W aircraft [14, 15]. In collaboration with Cranfield Aerospace and the U.S. Air Force Research Laboratory, NASA and Boeing extensively flight tested scale models of potential BWB configurations [16]. They pushed the flight vehicles to the edges of the flight envelope, particularly in the low-speed flight regimes. A challenge inherent to BWBs is containing pressure loads in a passenger cabin with a noncircular cross section. The PRSEUS project, carried out by NASA and Boeing, tested a possible solution of combining the skin, stringers, and frame into a single composite structure [17].

While the T&W configuration has become standard for transport aircraft, hydrogen's unique storage requirements may incentivize new configurations in ways kerosene has not. A hydrogen blended wing body (BWB) configuration (Figure 1b) is often suggested as a promising solution because it can efficiently package large hydrogen tanks. Airbus proposed a hydrogen BWB concept in 2020 [18], pointing to its large storage area. For the same reason, JetZero argues that there is a compelling case for a hydrogen-powered BWB [15]. Winnefeld et al. [19] speculate that BWBs enable more flexible hydrogen tank integration than a conventional T&W configuration, which could make them a desirable hydrogen aircraft configuration. Wilod Versprille [20] studies LH_2 tank packaging in a BWB, but does not draw conclusions about the impact of tank packaging on the BWB's performance.

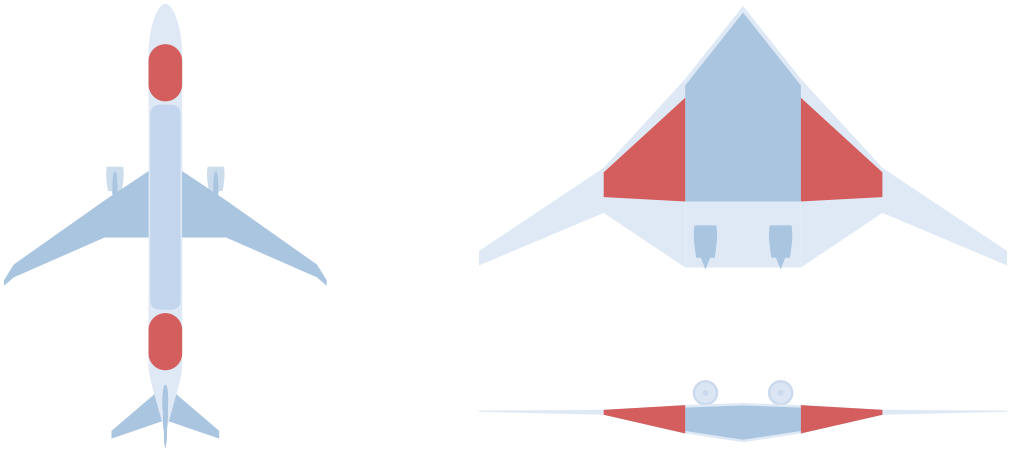

(a) Hydrogen T&W **(b) Hydrogen BWB**

Fig. 1 Most hydrogen T&W concepts store hydrogen in tanks at the front and rear of the fuselage, which adds weight and drag. The blended wing body configuration may be able to store the hydrogen more efficiently in large interior volumes where the cabin and wings blend together.

Researchers have yet to quantify the benefit of the BWB configuration compared to T&W for hydrogen-powered aircraft. In this work, we seek to answer that question by optimizing kerosene- and hydrogen-powered versions of each configuration using our conceptual aircraft design tool. For each configuration, we quantify the change in energy consumption, a fuel-agnostic efficiency metric, when the design is adapted from kerosene to hydrogen. By comparing the BWB's change in energy usage to the T&W's, we can determine if switching to hydrogen incentivizes the adoption of the BWB configuration.

II. Methodology

The goal of this work is to compare how liquid hydrogen storage requirements affect the energy usage of T&W and BWB airplane configurations. To do this, we optimize four aircraft concepts: a kerosene-powered T&W, a hydrogen-powered T&W, a kerosene-powered BWB, and a hydrogen-powered BWB. We compare the energy usage of each hydrogen-powered airplane to the kerosene-powered version of the same configuration to investigate how switching to hydrogen fuel affects each configuration's energy consumption.

The T&W and BWB configurations employ different modeling approaches that may overpredict or underpredict reality. Therefore, comparing the energy consumption of the hydrogen BWB directly to the kerosene T&W would raise more questions than answers. Higher fidelity models would be necessary for a direct fuel burn comparison between the two configurations, particularly given the limited empirical BWB data available. Instead of a direct comparison, we study the relative performance of each configuration's hydrogen-powered version to its kerosene-powered counterpart. This compensates for some of the modeling error.

The design mission is 5,500 nmi with a payload of 116,000 lbs (a maximum of 420 passengers), which is approximately the Boeing 787-9's maximum range at its maximum payload [21]. Cruise is at Mach 0.8 and 35,000 ft. The mission fuel includes the fuel from the takeoff, climb, cruise, and descent phases. The total fuel required includes the mission fuel plus the fuel for a 200 nmi reserve mission and 30 min loiter. The total fuel also includes an additional 6% to account for variability in engine performance and unreachable fuel [22]. The mission profile is shown in Figure 2.

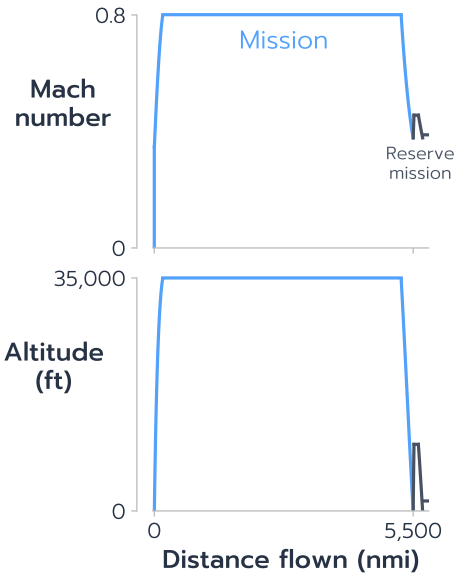

Fig. 2 The design mission is 5,500 nmi with a 200 nmi reserve mission.

OpenConcept* [23], a conceptual aircraft design toolkit, performs the mission analysis and time integration. OpenConcept is built on OpenMDAO [24] to enable efficient derivative computation. These derivatives allow efficient solution of large optimization problems by harnessing the power of gradient-based optimization [25]. OpenConcept uses numerical integrators to integrate aircraft states, such as fuel burn, over a customizable mission profile. At each numerical integration point, it selects the correct lift coefficient and engine throttle to balance lift, drag, thrust, and weight. The mission analysis is solved all at once using a monolithic Newton solver that takes advantage of the built-in analytic derivatives. The toolkit can handle complexity ranging from models with a simple parabolic drag polar and propulsion model to models using vortex lattice-based aerodynamics, hybrid-electric engine maps, and unsteady modeling of a battery and electric motor thermal management system.

The remaining portions of this section describe the methods used to model the T&W and BWB configurations, along with a validation case of the models.

*https://github.com/mdolab/openconcept

A. Tube and wing

An OpenConcept airplane model must compute weight, drag, and thrust as a function of lift coefficient, throttle, and flight conditions. Empirical relations estimate the T&W's weight. The drag prediction employs a combination of empirical textbook drag buildup methods and a physics-based vortex lattice code. A one-dimensional engine cycle model provides the thrust and fuel flow. The initial parameters are based on the Boeing 787-9.

1. Weight estimation

The in-flight weight is the sum of the fuel weight, payload weight, and operating empty weight. The fuel weight is computed by numerically integrating the fuel flow from the propulsion model and subtracting it from the initial fuel weight. The operating empty weight of the kerosene T&W aircraft is computed using empirical correlations. The wing, horizontal tail, vertical tail, fuselage, and landing gear weights are estimated by Raymer [22, Equations 15.25–15.30]. The maximum landing weight, an input to the landing gear weight, is computed by subtracting two thirds of the fuel weight from the maximum takeoff weight. Baseline engine, thrust reverser, engine control, and fuel system weights are computed using Wells et al. [26, Equations 76, 86, 87, and 92]. Correlations from Roskam [27, Equations 5.37 and 6.27] predict nacelle and engine starter weight. Furnishing and other equipment weights are also computed with Roskam [27, Equations 7.6, 7.15, 7.23, 7.29, 7.35, 7.40, and 7.44]. The structural weights, including the wing, tails, fuselage, landing gear, and nacelles, are multiplied by 1.2 to account for other miscellaneous items. The final operating empty weight is multiplied by an additional 1.15. With these factors held constant, the operating empty weight model predicts reasonable weight values for a wide range of transport aircraft.

A physics-based model estimates the cryogenic tank weight for the hydrogen T&W concept. The model assumes a vacuum-insulated aluminum tank construction because it is a promising tank design for future hydrogen aircraft [7]. The tank is cylindrical with two hemispherical endcaps. The vacuum-insulated tank has an inner shell that contains the pressure of the LH_2 inside the tank and separates the tank interior from the vacuum region. The vacuum region is enclosed by an outer shell that resists the compression of the external atmospheric pressure. The inner shell's thickness is sized by the hoop stress using

$$t_{\text{in}} = \frac{P_{\text{in}} r_{\text{in}} \gamma_{\text{in}}}{\sigma_{\text{yield, in}}}, \tag{1}$$

since the pressure of the tank's interior is greater than the pressure in the vacuum region. The maximum expected operating pressure (MEOP) of the tank is 2 bar, which is in the range of reasonable tank operating pressures [9, 28]. The outer shell is under compression because the atmospheric pressure on its exterior is greater than the pressure of the vacuum region. Thus, its thickness is sized to support buckling loads [28]. We use elastic buckling relationships for spherical and cylindrical shells under external pressure from Budynas and Sadegh [29, Table 15.2]:

$$t_{\text{out, sph}} = r_{\text{out}} \sqrt{\frac{P_{\text{out}} \gamma_{\text{out}}}{0.365E}}, \text{ and} \tag{2}$$

$$t_{\text{out, cyl}} = \left(\frac{P_{\text{out}} \gamma_{\text{out}} r_{\text{out}}^{1.5} L}{0.92E} \right)^{0.4}. \tag{3}$$

The outer thickness is the maximum of the thicknesses required for the spherical and cylindrical geometries multiplied by a factor f_{stiff} to account for the addition of stiffeners, which Sullivan et al. [28] show can substantially decrease the outer shell's weight. The parameters used for these calculations are listed in Table 1. The tank weight is then computed for each shell by multiplying its thickness by its surface area and material density. The final tank weight is multiplied by 1.1 to account for supports, plumbing, and other necessary equipment. For the hydrogen concepts, the operating empty weight is computed using the same models as the kerosene-powered concept and the hydrogen tank weight is added to the result.

The wing geometry is not suited to store the insulated cryogenic tanks for hydrogen aircraft [7]. Removing fuel from the wings eliminates the fuel load alleviation, which increases the weight of the wing structure. To account for this, we compare the wing weight relief factors provided by Jenkinson et al. [30] with and without the fuel weight load alleviation for a representative aircraft. Based on this estimate, we include a 20% wing weight penalty for the hydrogen concepts. The 20% weight penalty is a similar order to the penalty computed by performing steady aerostructural optimization with and without the fuel load alleviation [31].

Parameter	Value	Notes
P_{in}	200,000 Pa	MEOP of the internal tank
P_{out}	101,325 Pa	Representative maximum external pressure
γ_{in}	1.5	
γ_{out}	2.0	
$\sigma_{\text{yield, in}}$	413.7 MPa	Al 2014-T6 yield stress [28, Table IV]
E	80 GPa	LiAl 2090 Young's modulus [28, Table XIII]
ρ_{in}	2,796 kg/m^3	Al 2014-T6 density [28, Table IV]
ρ_{out}	2,699 kg/m^3	LiAl 2090 density [28, Table XIII]
f_{stiff}	0.8	

Table 1 Hydrogen tank structural parameters

2. Aerodynamics

We use a vortex lattice code to model the wing aerodynamics and textbook methods to estimate the drag of other components. The vortex lattice implementation is OpenAeroStruct [32], which is written using the OpenMDAO framework and provides analytic derivatives. OpenAeroStruct estimates parasitic drag with a flat-plate skin friction estimate and a form factor correction. It estimates wave drag with relations based on the Korn equation [33]. It is integrated into OpenConcept using a surrogate model [34]. Whenever the wing geometry changes, OpenConcept's surrogate model reruns OpenAeroStruct to generate a new surrogate model. The OpenAeroStruct mesh for the T&W concept is shown in Figure 3.

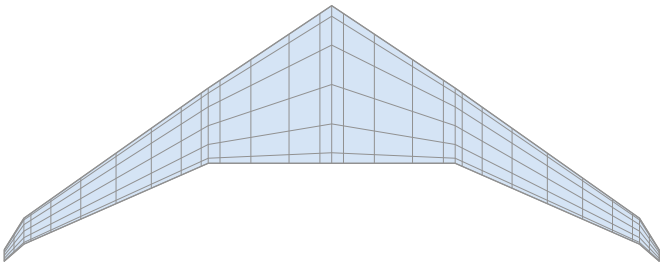

Fig. 3 The OpenAeroStruct mesh used for the T&W configuration.

An empirical drag buildup[†] is used to account for the drag of components other than the wing. The fuselage, horizontal tail, vertical tail, and nacelles use empirical form factor relations from Torenbeek [35] and interference factors from Raymer [22]. Skin friction coefficients are then computed for each of the components based on their characteristic length and the flight conditions. The drag coefficient of each component is computed by multiplying the form factor by the interference factor and skin friction coefficient. The resulting drag coefficients are renormalized by the wing planform area and added to the total drag coefficient. On takeoff, flaps and landing gear are extended which add drag. We add 200 drag counts to account for the extended landing gear [22]. Flap drag is computed using a curve fit of Roskam [36] estimates for Fowler flaps.

The maximum lift coefficient in the takeoff configuration is needed to estimate the takeoff field length. The clean maximum lift coefficient is based on an empirical relation from Raymer [22, Equation 12.15] between the two-dimensional airfoil maximum lift coefficient and the sweep angle. The clean two-dimensional airfoil maxmimum lift coefficient is 1.6. Extending the flaps and slats increases the maximum lift coefficient, which is modeled using correlations for Fowler flaps and slats from Roskam [36]. Takeoff flap deflection is assumed to be 10 degrees.

[†]The parasitic drag estimations are synthesized here: `https://openvsp.org/wiki/doku.php?id=parasitedrag` (accessed April 24, 2023)

3. Propulsion

We use a CFM56 engine model adapted from Adler et al. [37], which uses a surrogate model of the pyCycle [38] CFM56 engine model. To match more modern engines, we assume a 20% TSFC improvement. We have modified it to use hydrogen by assuming the same thrust-specific energy consumption (TSEC) as the kerosene-powered version, which offers a reasonable estimate of hydrogen fuel consumption [2, 7, 39]. The engine's thrust and fuel flow are linearly scaled to match the desired engine rating while maintaining the same TSFC.

4. Geometry and hydrogen tank integration

For the T&W concept, the fuselage is extended by the total length of the two hydrogen tanks to accommodate them without sacrificing passenger capacity. The stretched fuselage length is then used for all calculations. To maintain an appropriate rotation angle and capture trends in landing gear weight, the landing gear height is scaled by the ratio of the extended fuselage length to the original fuselage length.

The geometric design variables are shown in Figure 4. The wing area uniformly scales the entire wing. This links wing area to span, which may incentivize increasing the area to reduce induced drag. Wing twist controls the twist at the wing break and two outboard sections, linearly interpolating in between. The tank radius and length are also controlled by the optimizer. Both tanks have the same geometry.

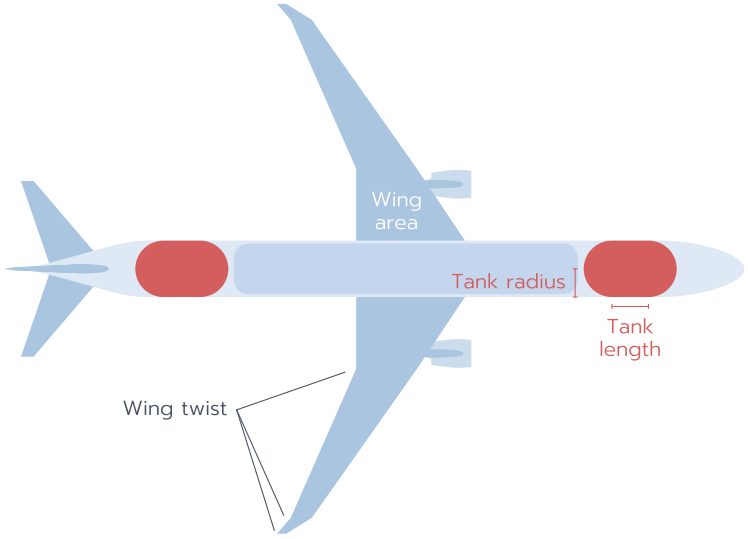

Fig. 4 The T&W geometry parameterization.

The vertical and horizontal tail areas are computed using tail volume coefficients [22, Equations 6.26 and 6.27]. The tail lever arm is assumed to be half the fuselage length. Other geometry parameters for the T&W concepts are taken from the Boeing 787-9.

5. Optimization problem

The T&W optimization, listed in Table 2, minimizes the mission fuel burn by varying the wing area, turbofan rated thrust, hydrogen tank geometry, and wing twist. The wing's planform geometry is based on the Boeing 787's wing to be representative of modern sweep, aspect ratio, and taper ratio values. The thickness-to-chord ratio of the wing ranges from 13.4% at the root to 10% at the tip. Twist is controlled at three spanwise stations, and the root is locked to prevent rigid body rotations of the wing. The hydrogen tank radius is bounded to ensure it fits within the fuselage. For the hydrogen T&W concept, we assume two equally-sized hydrogen tanks at the front and rear of the fuselage. This offers more center of gravity control than a single tank at the back of the fuselage.

The optimization is constrained so that the hydrogen tank is large enough to store the fuel required for the mission. The tank is not allowed to exceed a fill level of 95% because there must always be some room for the LH_2 to boil off to avoid drastic increases in tank pressure [7, 28]. The takeoff field length is computed using the method described by Brelje and Martins [23]. It is constrained to be less than 9,000 ft, in line with the Boeing 787-9 on a standard day at sea

level and MTOW [21]. Finally, the throttle must remain between 1 and 100% throughout the mission, which prevents the optimizer from selecting an engine that cannot meet the thrust requirements. This same throttle constraint could be accomplished by directly bounding the throttle in OpenConcept's Newton solver. However, allowing OpenConcept's Newton solver to select throttle values up to 120% and then constraining throttle to 100% in the optimization problem avoids analysis failures that slow the optimization by giving the optimizer more information.

We also use the optimizer to solve for the maximum takeoff weight by adding a constraint that the takeoff weight must be at least the sum of empty weight, payload weight, and fuel weight. Doing this removes an internal solver feedback loop, which reduces the overall optimization time and improves the Newton solver's robustness.

minimize	$W_{\text{mission fuel}}$
with respect to	Engine rated thrust
	Wing area
	Wing twist
	Hydrogen tank radius[‡]
	Hydrogen tank length[§]
	MTOW
subject to	0% ≤ hydrogen tank fill level ≤ 95%[¶]
	Takeoff field length ≤ 9,000 ft
	1% ≤ throttle ≤ 100%
	OEW + W_{payload} + $W_{\text{total fuel}}$ ≤ MTOW

Table 2 Optimization problem for T&W aircraft

We use SNOPT [40] through the pyOptSparse [41] interface. All optimizations are converged to an optimality tolerance of 10^{-6} and feasibility tolerance of 10^{-8}, providing a decrease in optimality from the baseline of roughly five orders. The optimizations take 5–10 min on a desktop computer with an AMD Ryzen 9 5950X.

B. Blended wing body

To model the BWB, we divide the geometry into three regions, shown in Figure 5. The center region is called the *centerbody*, and it contains a pressurized region for the passengers. Just outboard of the centerbody is the *blending region*, which stores the fuel for the hydrogen concepts. Finally, there is a higher aspect ratio wing outboard of the blending region. The combination of the furthest outboard wing and the blending region is called the *outerwing*. The outerwing stores fuel for the kerosene concept. The reason for storing hydrogen in the blending region rather than the whole outerwing is because a tank in the thinner outboard wing would have too high a surface area-to-volume ratio to efficiently accommodate the cryogenic LH_2 [7]. The absolute thickness of the blending region is greater, so it is possible to package tanks that are well suited to LH_2 storage. Unless otherwise specified in this section, the BWB concepts use the same models as the T&W concepts.

1. Weight estimation

The structural weight model is the only difference in weight estimation from the T&W. The fuselage, horizontal tail, and vertical tail are replaced by the centerbody, which is divided into two regions: the pressurized cabin and the unpressurized portion aft of the cabin. The weight of both of these regions is estimated using empirical correlations derived from finite element analyses by Bradley [42, Section 4.2]. The outerwing weight is computed using the same wing weight estimate as for the T&W.

We find that storing the hydrogen in one cylindrical tank with hemispherical endcaps in each blending region is not feasible (see Section II.B.4). Thus, we use conformal tanks that fill the region between the front and rear wing spars.

[‡]Tank radius is included only for the hydrogen T&W

[§]Tank length is included only for the hydrogen T&W

[¶]Fill level constraint is included only for the hydrogen T&W

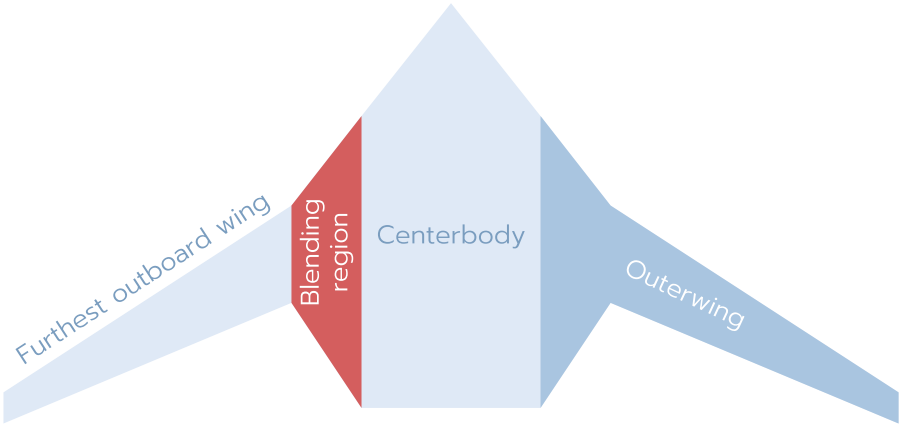

Fig. 5 The BWB geometry is defined by three linearly-varying regions.

Developing a physics-based structural model of a vacuum-insulated conformal LH_2 tank is difficult at low fidelity, so we assume a similar baseline gravimetric efficiency as the physics-based cylindrical tank model of 60% and investigate the sensitivity of the results to this value in Section IV. Gravimetric efficiency represents the fraction of the tank's total weight taken up by fuel when filled. It is written as

$$\eta_{\text{grav}} = \frac{W_{\text{fuel}}}{W_{\text{tank}} + W_{\text{fuel}}}, \tag{4}$$

where W_{fuel} is the maximum fuel weight the tank can hold and W_{tank} is the weight of the tank structure. A gravimetric efficiency of 60% is predicted to be feasible for vacuum-insulated cylindrical or spherical tanks [43], but is a rather ambitious target for conformal tanks. For example, Collins Aerospace is targeting a gravimetric efficiency of 35% for a variable section box-shaped LH_2 tank [44].

2. Aerodynamics

Unlike a T&W aircraft, a BWB's aerodynamics are dictated almost entirely by the wing. However, the wing has a significantly different shape than conventional wings, which are often nearly trapezoidal. OpenAeroStruct provides a cheap aerodynamic model that can capture the planform geometry changes of a BWB's unconventional wing shape. The mesh (Figure 6) estimates the lift and drag with errors of 0.1% and 1%, respectively, compared to a mesh with 20 times the number of panels. The BWB wave drag estimation is based only on the outerwing geometry, similar to the approach taken by Kays [45], rather than OpenAeroStruct's default of using the whole wing. Other than the wing drag, the nacelles are the only other parasitic drag source modeled in flight using the same approach as the T&W. Because we do not account for pitching moment trim in the planform and twist optimization, an extra 5% drag penalty is added. This is roughly equal to the difference in drag between BWBs optimized with and without a pitching moment constraint found by Lyu and Martins [46].

On takeoff, the landing gear drag is added. The landing gear drag coefficient of 0.02 is halved because it is now normalized by roughly twice the planform area. Trailing edge flaps are excluded because the BWB has no tail to trim the pitching moments they produce [13]. The BWB also has a lower wing loading than conventional aircraft because of the additional lifting area the centerbody provides, which means it has adequate high lift performance and flaps are unnecessary [46].

The maximum lift coefficient for the BWB is estimated using the critical section method. This approach determines the largest angle of attack where all sectional lift coefficients are less than or equal to their maximum two-dimensional airfoil lift coefficient. The wing's lift coefficient at that angle of attack is taken to be the maximum lift coefficient. High-lift design for BWBs is still an active area of research, so we assume a maximum sectional lift coefficient value of 1.7. The angle of attack is solved using OpenMDAO's nonlinear Schur complement solver [47], which circumvents the need to assemble and solve a linear system that contains the entire OpenAeroStruct vortex lattice model. Using the Schur solver decreased the run time of the maximum lift coefficient solve for our problem by a factor of 20 compared to using a Newton solver.

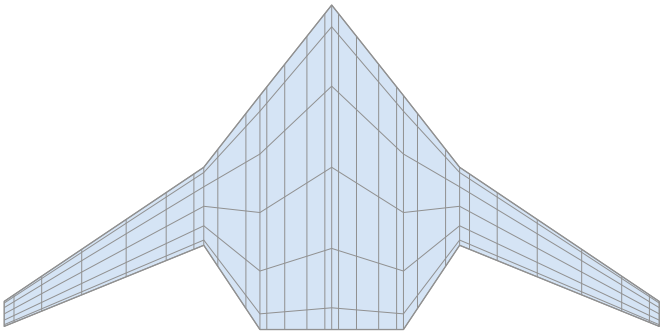

Fig. 6 The OpenAeroStruct mesh used for the BWB configuration (initial planform geometry).

3. Propulsion

The BWB uses the same engine model as the T&W configuration with the same methods of adapting to hydrogen fuel and variable engine ratings.

4. Geometry and hydrogen tank integration

The baseline BWB geometry is designed to provide a comparable cabin floor area to the Boeing 787-9's cabin. The initial centerbody and outerwing planform shape is chosen to align with designs from Boeing [13], MIT [45, 48], JetZero[‖], and other similar concepts. We assume the pressurized passenger cabin extends from the leading edge to the rear spar, which is located at 65% chord in the outerwing and extends straight through the centerbody. The front spar is at 10% chord in the outerwing.

We initially attempt to package a single cylindrical LH_2 tank with hemispherical endcaps into each blending region, shown in Figure 7. With our parameterization, the blending region could not be made big enough to fit sufficiently large tanks. A BWB with cylindrical LH_2 tanks may be feasible with a different packaging solution, geometry parameterization, or multiple cylindrical tanks in each blending region.

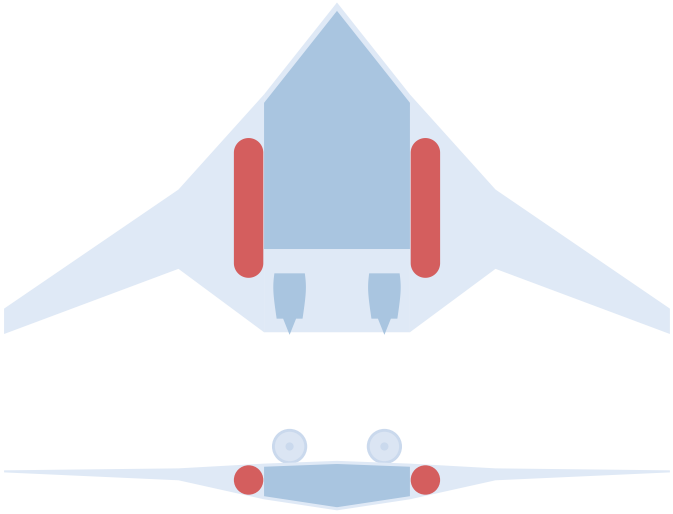

Fig. 7 The blending regions do not have enough volume to store the necessary hydrogen with a single cylindrical tank on each side. The tanks in this figure containly only half of the hydrogen needed to fly the mission. A more refined geometry parameterization could potentially make this configuration feasible.

[‖] `https://www.jetzero.aero/` (accessed April 24, 2023)

Because cylindrical LH_2 tanks do not fit, we consider conformal tanks that fill the space in the blending region between the front and rear spars (Figure 8). The volume of these tanks is computed by integrating the thickness from 10–65% chord of a NASA SC(2)-0412 airfoil scaled to match the thickness-to-chord ratios of the inner and outer blending region sections. The tanks are formed by linearly lofting between the two airfoil sections and integrating to compute the total tank volume.

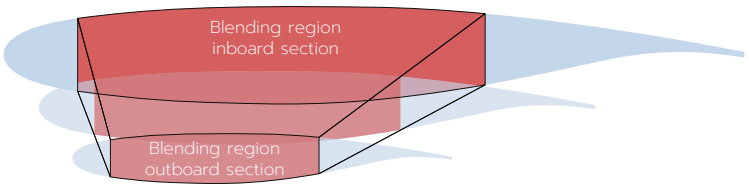

Fig. 8 The conformal tank volume is computed by integrating the cross sectional area at the inboard in outboard blending region sections and linearly lofting them.

The BWB geometry parameterization must give the optimizer enough freedom to shape the blending region to store the hydrogen tanks and capture the important packaging tradeoffs.** Physical considerations such as structural design and important three-dimensional flow field effects are missing from the low-fidelity model. Thus, the parameterization and geometry constraints must also be restrictive enough to obtain reasonable designs.

The parameterization for this work, shown in Figure 9, locks the centerbody planform geometry and thickness-to-chord ratio (set to a constant 15%). The optimizer can vary the thickness-to-chord ratio, chord, spanwise position, and streamwise position of the outboard blending region section. It can also change the spanwise position of the outermost wing section. The taper ratio, quarter chord sweep angle, and tip thickness-to-chord ratio of the furthest outboard wing region is held constant. The aspect ratio of the furthest outboard wing region and the streamwise position of the quarter mean aerodynamic chord are constrained to account for structural and stability considerations.

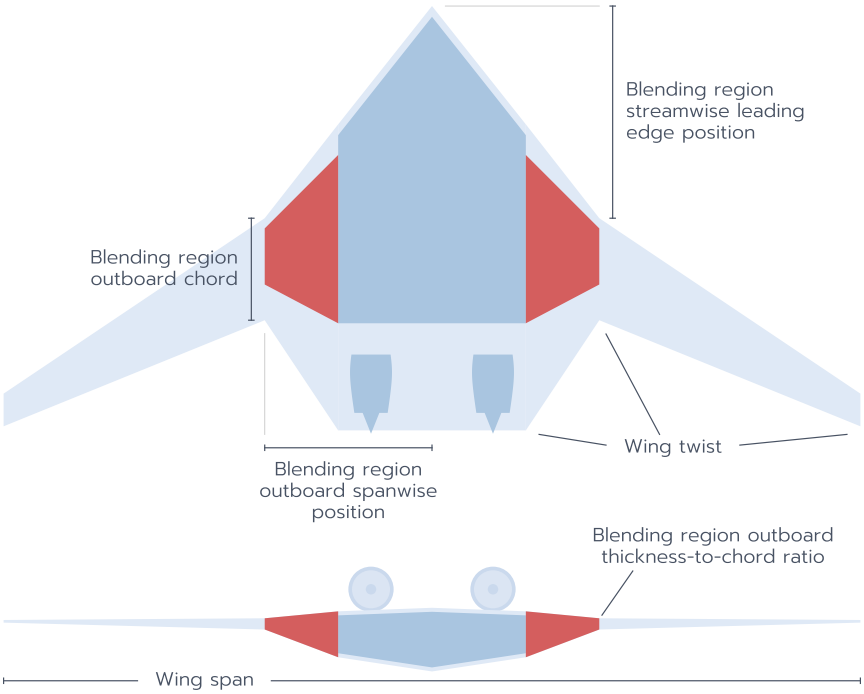

Fig. 9 The BWB geometry parameterization focuses design freedom around the blending region.

**For example, if the optimizer can adjust the blending region width but not the width of the furthest outboard wing, it widens the blending region to increase the overall span. This makes the blending region artificially large and reduces the apparent penalty of packaging hydrogen tanks.

5. Optimization problem

The BWB optimization problem is the same as the one for the T&W aircraft, except that it replaces the T&W's geometric design variables with the corresponding BWB parameters, described in Section II.B.4. The lower bound on blending region outboard thickness-to-chord ratio is 11%. The blending region outboard spanwise position is not allowed to encroach too closely on the outboard section of the centerbody (this is active for the optimizations without a hydrogen tank fill level constraint). The wing span is limited to be no greater than the baseline.

minimize	$W_{\text{mission fuel}}$
with respect to	Engine rated thrust
	Blending region outboard thickness-to-chord ratio
	Blending region outboard chord
	Blending region outboard spanwise position
	Blending region outboard streamwise leading edge position
	Wing span
	Wing twist
	MTOW
subject to	0% ≤ hydrogen tank fill level ≤ 95%[††]
	Change in streamwise quarter MAC position = 0
	Furthest outboard wing aspect ratio ≤ 10
	Takeoff field length ≤ 9,000 ft
	1% ≤ throttle ≤ 100%
	OEW + W_{payload} + $W_{\text{total fuel}}$ ≤ MTOW

Table 3 Optimization problem for BWB aircraft

C. Validation

We validate our approach by modeling a Boeing 787-9 flying a 5,250 nmi mission with maximum payload and comparing to the true values [21]. This mission corresponds to the 787-9's maximum range at maximum payload. Because we don't know the twist of the 787, we obtain the values for validation by performing a twist-only optimization that minimizes fuel burn. The validation results are shown in Table 4.

Parameter	**Boeing 787-9 [21]**	**OpenConcept**	**OpenConcept error**
MTOW (lb)	560,000	551,155	−1.6%
OEW (lb)	280,000	281,739	0.6%
Total fuel (lb)	160,000	161,475	0.9%
Takeoff field length (ft)	9,300–9,900[‡‡]	7,938	−14.6 to −19.8%

Table 4 Boeing 787-9 validation on a 5,250 nmi at maximum payload.

[††] Fill level constraint is included only for the hydrogen T&W

[‡‡] Takeoff field length varies with different engine options

III. Results

In this section, we investigate the results of the optimizations. We first analyze the two T&W aircraft and explain key differences in the optimized designs. Then we do the same for the two BWB aircraft. Finally, we study how each configuration adapts to hydrogen fuel by comparing each configuration's change in energy usage from the kerosene to the hydrogen version.

The optimized T&W aircraft are shown in Figure 10. Packaging the hydrogen tanks results in a longer fuselage, which increases the fuselage drag in cruise by 24%. The stretched fuselage has a length-to-diameter ratio similar to the Boeing 757-300's fuselage. Lengthening the fuselage increases the moment arm of the tail, which enables smaller horizontal and vertical stabilizers.

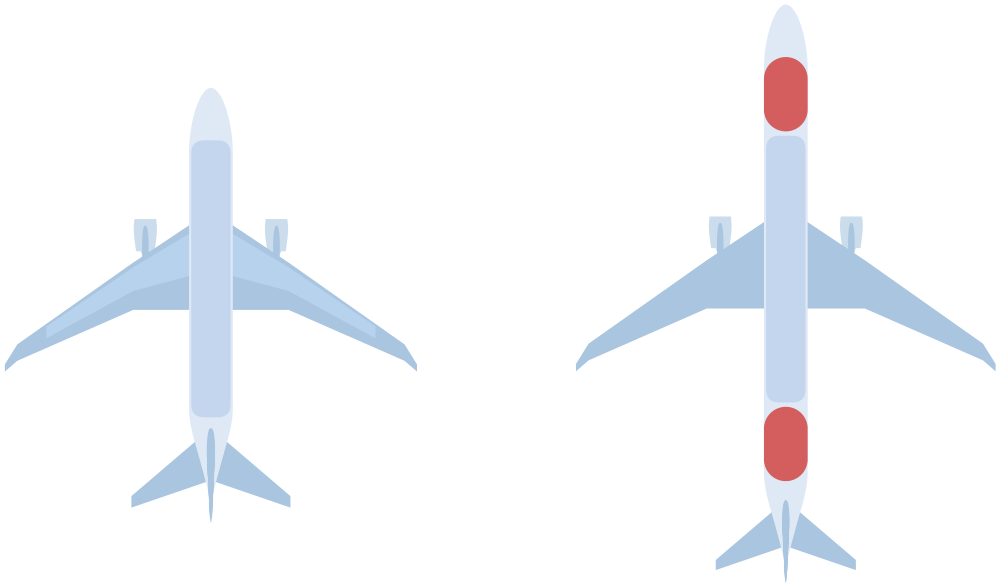

(a) Optimized kerosene T&W **(b) Optimized hydrogen T&W**

Fig. 10 Compared to the optimized kerosene T&W, the hydrogen T&W has a 4% larger wing area, 4% less powerful engines, and a 36% longer fuselage to accommodate the tanks.

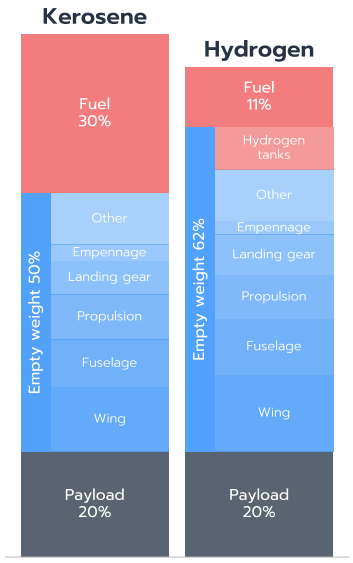

Fig. 11 The optimized hydrogen T&W has a lower MTOW but greater OEW than the kerosene version.

The longer fuselage and addition of the hydrogen tanks increase the operating empty weight of the hydrogen T&W compared to the kerosene version. The longer fuselage also requires taller landing gear to achieve the same rotation angles, which increases the landing gear weight by 22%. Despite the greater empty weight, the hydrogen-powered concept's MTOW is 7% less than the kerosene concept's (Figure 11). This is because hydrogen carries three times the energy of kerosene in the same weight, so the fuel weight is reduced by a factor of three. The lighter takeoff weight allows the optimizer to shrink the engines. The lower MTOW also means that the maximum lift force the wing must produce is lower. This reduced lift force and slightly offsets the 20% wing weight penalty from the lack of fuel load alleviation, but the wing is still 19% heavier than the kerosene aircraft's wing.

Figure 12 shows the optimized BWB aircraft. The optimizer collapses the blending region of the kerosene-powered BWB as much as the design variable bounds allow. This change shrinks the wetted area, reducing drag. The optimizer also lowers the thickness-to-chord ratio of the blending region's outboard section to the lower bound of 11%. The span extends to the design variable's upper bound to reduce induced drag. Finally, the chord of the blending region's outboard section shrinks, further reducing wetted area and drag, until the takeoff field length constraint prevents further reduction. A smaller wing would not be able to provide enough lift to takeoff in the required distance.

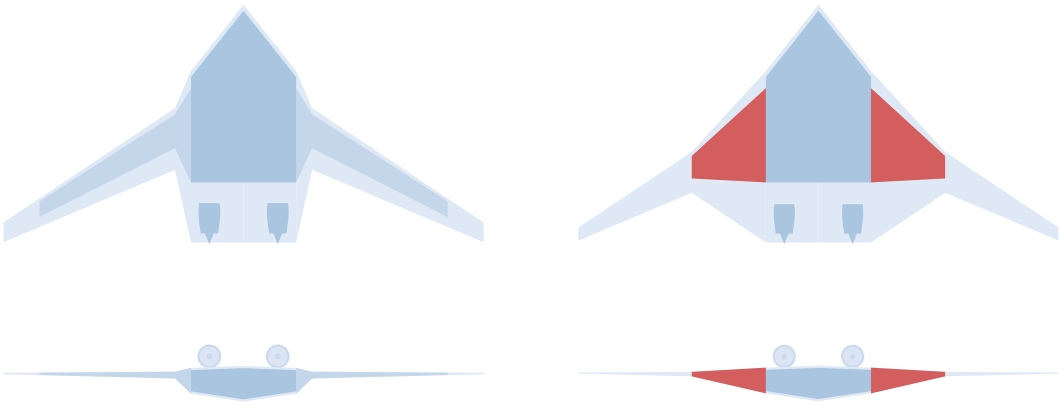

(a) Optimized kerosene BWB **(b) Optimized hydrogen BWB**

Fig. 12 The kerosene BWB collapses the blending region to decrease wetted area, while the hydrogen version widens the blending region so it can store enough fuel.

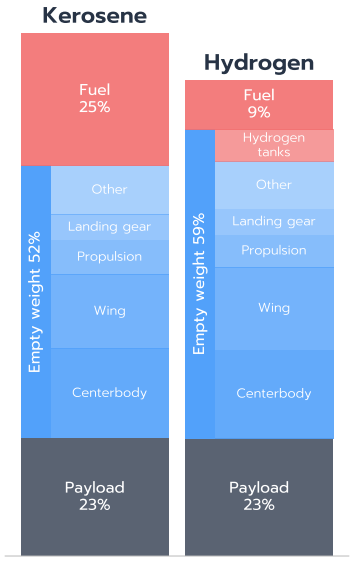

Fig. 13 The optimized BWB weight breakdowns show similar trends to the optimized T&W aircraft.

The hydrogen BWB takes on a very different shape than the kerosene BWB because the blending regions must be large enough to store the hydrogen. Due to the larger blending regions, the wetted area is 10% greater than the kerosene BWB's. Despite its starkly different shape and greater planform area than the kerosene BWB, the hydrogen BWB achieves a 9% reduction in MTOW compared the the kerosene BWB (Figure 13). The hydrogen BWB's wing is 12% heavier than the kerosene BWB's. Some of the 20% wing weight penalty from the lack of fuel load alleviation is compensated by the smaller aspect and taper ratios, along with the lower lift force required because of the hydrogen BWB's reduced takeoff weight.

The aim of this work is to determine whether T&W aircraft or BWBs more efficiently adapt to hydrogen aircraft requirements. We measure the efficiency of converting a configuration to hydrogen by comparing the energy usage of the hydrogen and kerosene versions of each configuration. A lower ratio of the hydrogen aircraft to kerosene aircraft's energy consumption indicates a concept that is better suited to hydrogen storage. The result does not determine which configuration uses less energy; it only describes whether having to store hydrogen tilts the scales in favor of one of the configurations. This is because we compare each hydrogen aircraft only to the kerosene aircraft with the same configuration. We do not compare, for example, the hydrogen BWB's energy usage directly to the kerosene T&W's.

Figure 14, shows the difference in energy usage between the hydrogen and kerosene T&W aircraft, while Figure 15 shows the same plot for the BWB. The conversion from kerosene to hydrogen is broken into three steps to offer additional insights into the source of the differences between the two configurations. The design is optimized at each step with the appropriate design variables and constraints. The differences between the steps are the following:

1) **Switch to hydrogen:** Account for the higher specific energy of hydrogen, which results in a 2.8 times lower TSFC. Because there is no longer kerosene stored in the wings, include the 20% wing weight penalty.
2) **Include tank weight:** Include the hydrogen tank weight in the empty weight calculation. For the T&W, this requires adding tank radius and length design variables along with the fill level constraint to the optimization. However, the fuselage is not lengthened to account for the tank packaging. For the BWB, the tank weight calculation does not require any knowledge of the tank geometry, so the fill level constraint is still left out of the optimization problem.
3) **Include tank integration:** Package the hydrogen tank into the airframe. For the T&W, stretch the fuselage to fit the tanks. Stretching the T&W's fuselage also involves lengthening the its landing gear. For the BWB, add the fill level constraint to the optimization, which forces the optimizer to make the blending region large enough to store the required hydrogen.

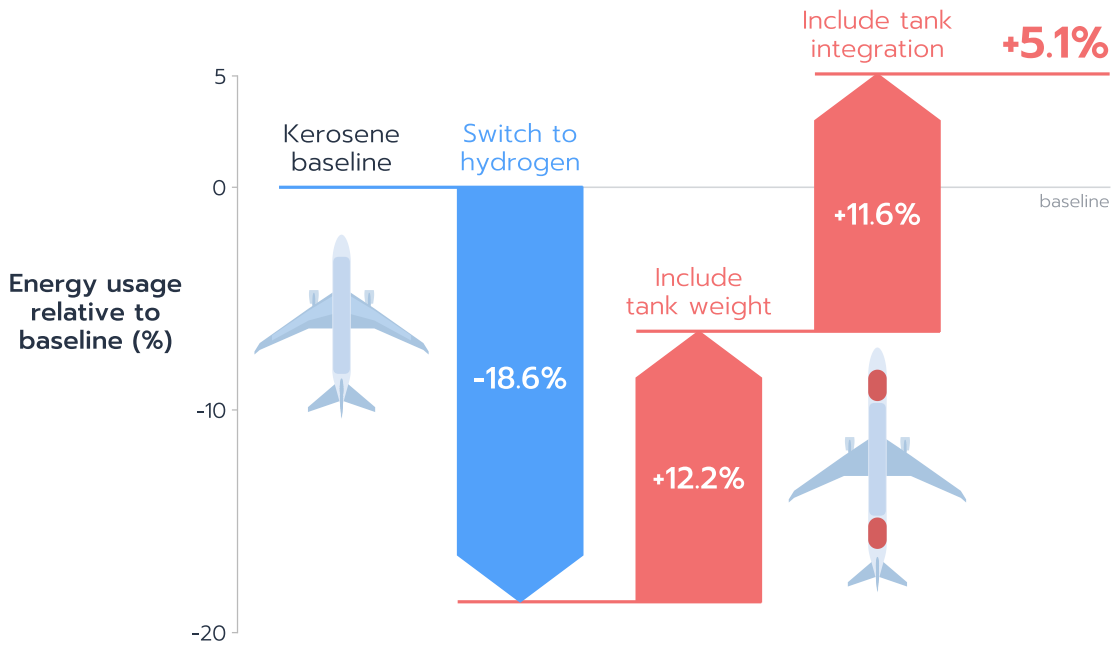

Fig. 14 The reduction in fuel weight from hydrogen's greater specific energy than kerosene is counteracted by the tank weight and integration penalties. This results in a net energy consumption increase of 5.1% for the hydrogen-powered T&W aircraft compared to the kerosene-powered baseline.

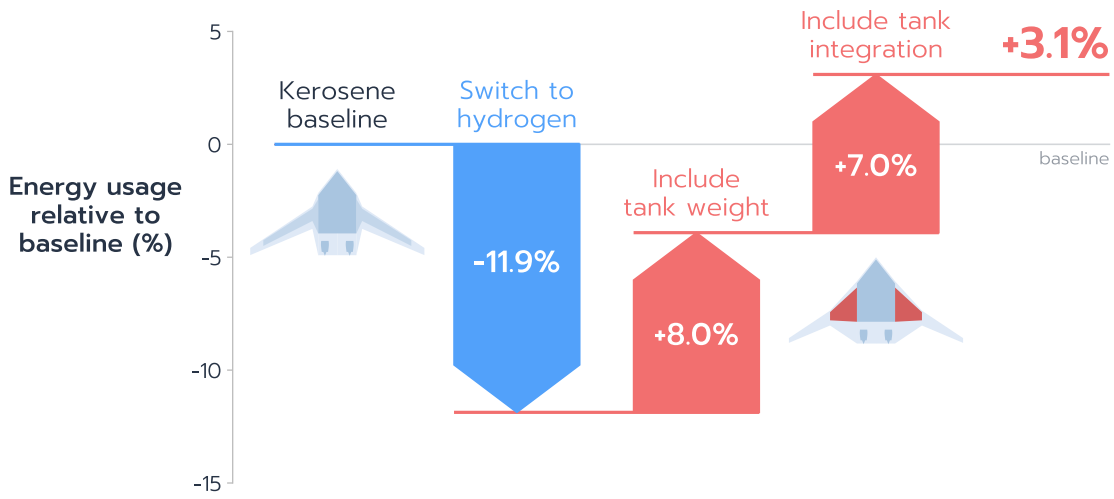

Fig. 15 The BWB benefits less from switching to hydrogen than the T&W because of its lower fuel fraction. After including the tank weight and integration penalties, the hydrogen-powered BWB uses 3.1% more energy than the kerosene-powered baseline.

Switching the T&W concept to hydrogen reduces energy consumption by 18.6%, while the BWB saves only 11.9% energy. This difference is due to a combination of factors. One cause is that the BWB concepts have a lower fuel fraction than the T&W aircraft, which is an effect of the BWB's greater aerodynamic efficiency. The lower fuel fraction means that the BWB's takeoff weight decreases less than the T&W's when the fuel weight is reduced by a factor of three. Another source of the difference is that the wing is a greater fraction of the total weight for the BWB than the T&W. This means that the 20% wing weight penalty from the removal of fuel load alleviation hurts the BWB more than the T&W. A third cause is the indirect effect of switching to hydrogen on the T&W's tail sizing. Switching to hydrogen reduces the takeoff weight. The lower takeoff weight allows the wing to shrink. A smaller wing and lighter aircraft reduces the required size of the horizontal and vertical stabilizers. The horizontal and vertical stabilizers account for 6% of the kerosene T&W's empty weight and 9% of the drag in cruise, so reducing their size can have a significant effect on fuel burn. Because the BWB configuration has no tail, it misses out on these savings.

Adding the tank weight reduces the benefit of hydrogen for the T&W aircraft by two thirds. The 8% penalty in energy consumption from adding the tanks to the BWB is smaller than the T&W's. However, this increase is similar relative to the initial energy savings from switching to hydrogen. The smaller percent increase may be due in part to the higher aerodynamic efficiency, which results in smaller changes to fuel burn for a given change in weight and lighter tanks due to the lower fuel fraction.

Finally, integrating the hydrogen tanks into the T&W aircraft results in a net increase in energy consumption of 5.1% for the hydrogen-powered version compared to the kerosene-powered baseline. Lengthening the fuselage shrinks the horizontal and vertical tails, which reduces their weight and drag. On the other hand, the longer fuselage increases the fuselage's weight and drag. It also requires longer landing gear to maintain suitable rotation angles for takeoff and landing without striking the tail on the ground, which increases the landing gear weight. Adding the tank fill level constraint to the BWB increases the outerwing planform area by 35%, adding substantial wetted area that increases drag. This yields an energy increase of 3.1% compared to the kerosene BWB baseline.

For safety reasons, it may be required to store the liquid hydrogen tanks outside of the pressurized passenger cabin. The T&W would require two extra pressure bulkheads in the fuselage to accomplish this—one behind and one in front of the forward hydrogen tank. Assuming the two bulkheads add a total of 1,000 kg to the aircraft's weight, the new energy usage difference between the kerosene and hydrogen T&W concepts rises from 5.1% to 6.0%. This modification is speculative and meant to give only a rough idea of the potential impact of extra pressure bulkheads.

These results suggest that the BWB configuration may not be any better at adapting to hydrogen than the conventional T&W configuration. However, this conclusion does not rule out a hydrogen-powered BWB. If the kerosene BWB baseline uses, for example, 50% less energy than the kerosene T&W, a hydrogen BWB still has the potential to use far less energy than a hydrogen T&W. Additionally, the models are only a guess of reality so they are subject to uncertainty. We investigate the effects of this uncertainty in the following section.

IV. Sensitivity Analysis

This section investigates how the conclusions change when modeling assumptions are made more or less conservative. This offers insights into the robustness of the conclusions to model variability. We explore the sensitivity to the hydrogen tank weight, operating empty weight, and total drag. We also study how the results change when the BWB's conformal tank is extended to fill the entire blending region. The conclusions in the previous section are based on the energy of each configuration's hydrogen version relative to its kerosene version. Thus, we measure this metric's sensitivity to the variables of interest. The metric does not represent the absolute energy usage; insensitivity indicates that the hydrogen version's energy usage relative to the kerosene version's is constant, not that the energy usage itself is constant.

To examine the sensitivity of the results to the hydrogen tank weight (Figure 16), we apply multipliers to the tank weight estimates for the hydrogen version of each configuration. The resulting energy consumptions are compared to the kerosene-powered baselines. The point where the hydrogen and kerosene versions have similar energy consumptions is 65–70% for both configurations, though the T&W's crossover point is slight lower. The BWB's greater lift-to-drag ratio means that a weight increase adds less drag than it would for the T&W. Therefore energy consumption is also less sensitive to weight changes, and thus to gravimetric efficiency. This flattens the BWB's curve compared to the T&W's. However, the conformal tanks on the BWB likely have a lower gravimetric efficiency than the T&W's tanks. As discussed in Section II.B.1, this is because their shape does not contain pressure loads as well as the T&W's cylindrical tanks. This effect makes it more challenging for the BWB to compete with the T&W because the hydrogen BWB would fall further to the left on Figure 16 than the T&W would. Based on this sensitivity study, the conclusions are reasonably robust to to the tank weight model. If both configurations used tanks with substantially lower gravimetric efficiencies, the BWB configuration may have an advantage.

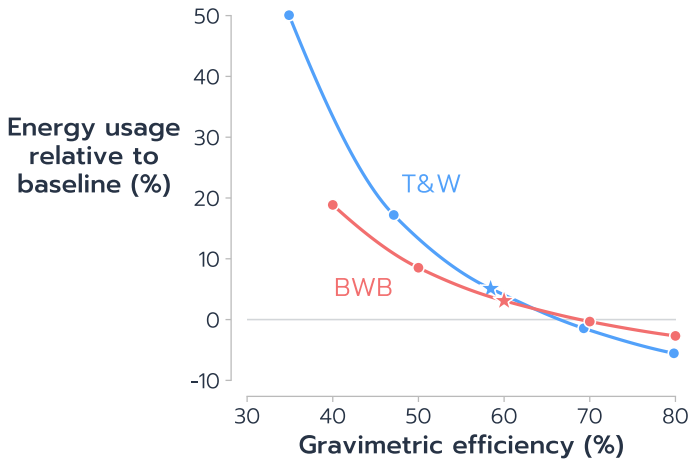

Fig. 16 The BWB's higher lift-to-drag ratio makes it less sensitive to weight changes. The star marks the gravimetric efficiency assumed in Section III.

To investigate the sensitivity to empty weight and drag, we apply a multiplier on the total empty weight and drag estimates for both the kerosene baseline and hydrogen aircraft. We compute the difference in energy consumption between the modified kerosene and hydrogen aircraft as we vary the multiplier's value. The results are shown in Figure 17. The difference in energy usage between the hydrogen and kerosene BWBs is nearly constant as the weight and drag models change. The T&W exhibits a very different trend. As weight and drag increase, the hydrogen T&W's energy usage increases relative to the kerosene T&W's. The T&W is particularly sensitive to empty weight.

The two configurations' dramatically different sensitivities to empty weight and drag are likely due to how each configuration responds to changes in fuel volume. When the T&W's empty weight increases, the wing area must also increase, adding weight. For the kerosene concept, the larger wing (and tail) is the only geometry change. However for the hydrogen concept, the hydrogen tanks and fuselage must be lengthened to store the fuel required to carry the additional weight. The longer fuselage adds both drag and weight, and it does not substantially contribute to the additional lift required. This difference between the hydrogen and kerosene T&Ws might be what causes the hydrogen T&W to become less competitive with the kerosene version as the empty weight model is made more conservative. On the other hand, the BWB's wing area increases as the hydrogen tank expands because the tank is contained in a lifting surface. Therefore, increasing the BWB's empty weight increases the wing area of both the kerosene and hydrogen

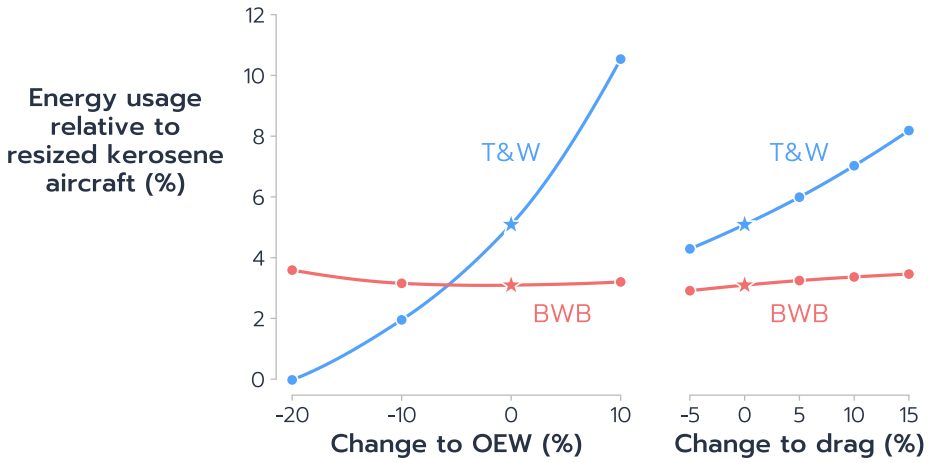

Fig. 17 The relative energy consumption of the hydrogen and kerosene BWBs is far less sensitive than the T&Ws to changes in the weight and drag models. The star marks the weight and drag assumed in Section III.

versions. The hydrogen BWB's larger wing can already contain more hydrogen fuel, so the BWB does not experience the same penalty from extending the fuselage as the T&W does. The similar increases to wing area and weight likely explain the consistent energy consumption difference between the hydrogen and kerosene BWBs.

Finally, we extend the length of the conformal tanks to the full chord. This is the best case scenario for the BWB if all the fuel is stored in the blending regions. Figure 18 shows the optimized result with this tank configuration. Despite the noticeably smaller blending regions, this hydrogen BWB still uses 1.4% more energy than the kerosene BWB. This is likely due to the way the conformal tank volume is computed (Figure 8). The tank's cross sectional areas at the inboard and outboard sections are computed by integrating the area of a supercritical airfoil at the tank's chordwise positions. Most of the airfoil's area is in the first half of the chord. Thus, even though the chord of the tank is nearly doubled by this modification, the airfoil area taken up by the tank increases only 33%. The result is only a limited improvement in the hydrogen BWB's energy consumption relative to the kerosene BWB baseline.

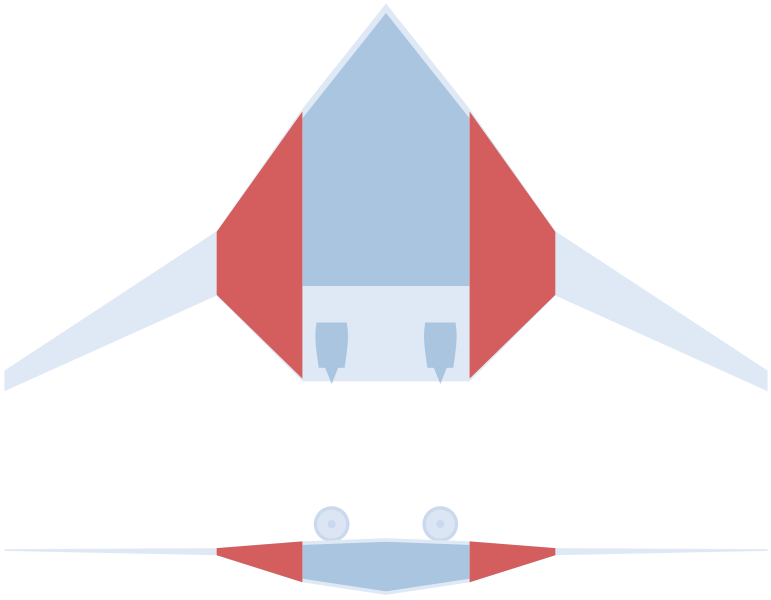

Fig. 18 Even when the BWB's conformal tank is stretched to fill the entire blending region, it stills uses 1.4% more energy than the kerosene BWB.

V. Conclusion

We investigate the argument that the BWB configuration naturally lends itself to being powered by hydrogen because it can efficiently store large volumes of hydrogen fuel. To do this, we design kerosene and hydrogen versions of conventional T&W and BWB configurations. We determine how well each configuration adapts to hydrogen by comparing the energy consumption of the hydrogen version to the kerosene version of each configuration.

We find that the BWB configuration is only marginally better at adapting to hydrogen fuel than the conventional T&W configuration. The hydrogen BWB uses 3.1% more energy than the kerosene BWB baseline, even with ambitious conformal hydrogen tank gravimetric efficiency assumptions. The hydrogen T&W consumes 5.1% more energy than its kerosene T&W baseline. Hydrogen delivers the same energy as kerosene but with one third the weight. The kerosene BWB has a lower fuel fraction than the kerosene T&W, so the BWB does not benefit as much as the T&W from hydrogen's high energy per mass. The energy consumption penalty from integrating hydrogen tanks into the BWB is similar to the T&W's penalty relative to the amount each configuration benefits from hydrogen's high energy per mass.

We evaluate the robustness of these conclusions to uncertainty in the tank weight, empty weight, and drag models. The BWB results are less sensitive than the T&W's to all the variables we test. This is partially due to the BWB's greater lift-to-drag ratio, since it results in smaller thrust increases (and thus energy consumption) for a given increase in weight. But it is also due to the BWB's integration of the tanks into a lifting surface. When additional fuel is required, the T&W configuration's fuselage must be extended to make room for more tank volume. This adds drag and weight. The size of the wing must then increase to support the extra weight, which adds weight and drag, requiring more fuel, and so on. With the BWB, increasing the blending region size to contain more fuel already corresponds to an increase in wing area, so the net increase in energy consumption is not as high as for the T&W.

These results are intriguing and perhaps unexpected; more work should be done to understand the tradeoffs between the T&W and BWB configurations for hydrogen-powered aircraft. While the hydrogen storage location in the T&W is fairly straightforward, the BWB offers a wide range of tank integration possibilities. Future work should investigate alternative tank packaging solutions, particularly in an aerodynamic shape optimization context, while including the impact of design decisions on aircraft sizing.

Acknowledgments

The first author is supported by the Department of Defense through the National Defense Science and Engineering Graduate (NDSEG) Fellowship Program. He is also supported in part by the Michigan Institute for Computational Discovery and Engineering (MICDE) Graduate Fellowship program. The authors would like to thank M. A. Saja Abdul-Kaiyoom for his help with the nonlinear Schur complement solver.

References

[1] Clean Sky 2 Joint Undertaking, and Fuel Cells and Hydrogen 2 Joint Undertaking, "Hydrogen-powered aviation: A fact-based study of hydrogen technology, economics, and climate impact by 2050," Report, Publications Office of the European Union, 2020. https://doi.org/10.2843/471510.

[2] Mukhopadhaya, J., and Rutherford, D., "Performance Analysis of Evolutionary Hydrogen-Powered Aircraft," , Jan 2022.

[3] Airbus, "Airbus reveals new zero-emission concept aircraft," https://www.airbus.com/en/newsroom/press-releases/2020-09-airbus-reveals-new-zero-emission-concept-aircraft, September 2020. Accessed March 16, 2022.

[4] Airbus, "Airbus and CFM International to pioneer hydrogen combustion technology," https://www.airbus.com/en/newsroom/press-releases/2022-02-airbus-and-cfm-international-to-pioneer-hydrogen-combustion, Feb 2022. Accessed July 18, 2022.

[5] Pratt & Whitney, "Pratt & Whitney Awarded Department of Energy Project to Develop Hydrogen Propulsion Technology," https://newsroom.prattwhitney.com/2022-02-21-Pratt-Whitney-Awarded-Department-of-Energy-Project-to-Develop-Hydrogen-Propulsion-Technology, Feb 2022. Accessed July 18, 2022.

[6] Rolls-Royce, "Rolls-Royce and easyJet set new world first," https://www.rolls-royce.com/media/press-releases/2022/28-11-2022-rr-and-easyjet-set-new-aviation-world-first-with-successful-hydrogen-engine-run, November 2022. Accessed February 18, 2023.

[7] Adler, E. J., and Martins, J. R. R. A., "Hydrogen-Powered Aircraft: Fundamental Concepts, Key Technologies, and Environmental Impacts," *Progress in Aerospace Sciences*, 2023. (In press).

[8] Onorato, G., Proesmans, P., and Hoogreef, M. F. M., "Assessment of hydrogen transport aircraft," *CEAS Aeronautical Journal*, Vol. 13, 2022. https://doi.org/10.1007/s13272-022-00601-6.

[9] Verstraete, D., Hendrick, P., Pilidis, P., and Ramsden, K., "Hydrogen fuel tanks for subsonic transport aircraft," *International Journal of Hydrogen Energy*, Vol. 35, No. 20, 2010, pp. 11085–11098. https://doi.org/10.1016/j.ijhydene.2010.06.060.

[10] Brewer, G. D., *Hydrogen Aircraft Technology*, CRC Press, Boca Raton, Florida, 1991.

[11] Cryoplane Project, "Liquid hydrogen fuelled aircraft—system analysis," Technical report GRD1-1999-10014, European Commission, September 2003.

[12] Debney, D., Beddoes, S., Foster, M., James, D., Kay, E., Kay, O., Shawki, K., Stubbs, E., Thomas, D., Weider, K., and Wilson, R., "Zero-Carbon Emission Aircraft Concepts," FlyZero report FZO-AIN-REP-0007, Aerospace Technology Institute, Mar 2022. URL https://www.ati.org.uk/wp-content/uploads/2022/03/FZO-AIN-REP-0007-FlyZero-Zero-Carbon-Emission-Aircraft-Concepts.pdf.

[13] Liebeck, R. H., "Design of the Blended Wing Body Subsonic Transport," *Journal of Aircraft*, Vol. 41, No. 1, 2004, pp. 10–25. https://doi.org/10.2514/1.9084.

[14] Bravo-Mosquera, P. D., Catalano, F. M., and Zingg, D. W., "Unconventional aircraft for civil aviation: A review of concepts and design methodologies," *Progress in Aerospace Sciences*, Vol. 131, 2022, p. 100813. https://doi.org/10.1016/j.paerosci.2022.100813.

[15] Page, M., and Vassberg, J., "BWB and the Climate," https://vimeo.com/747462950/1165b9e036 (accessed April 25, 2023), September 2022. Presented at the 33rd Congress of the International Council of the Aeronautical Sciences.

[16] Creech, G., "X-48B BWB Team Completes Phase 1 Test Flights," https://www.nasa.gov/centers/dryden/news/NewsReleases/2010/10-12.html, April 2010. Accessed 8 November 2022.

[17] Velicki, A., and Jegley, D., *PRSEUS Development for the Hybrid Wing Body Aircraft*, Aviation Technology, Integration, and Operations (ATIO) Conferences, American Institute of Aeronautics and Astronautics, 2011. https://doi.org/10.2514/6.2011-7025, URL http://arc.aiaa.org/doi/10.2514/6.2011-7025.

[18] Norris, G., "Airbus Reveals Refined ZEROe Blended Wing Body Concept," https://aviationweek.com/shownews/singapore-airshow/airbus-reveals-refined-zeroe-blended-wing-body-concept, February 2022. Accessed April 22, 2023.

[19] Winnefeld, C., Kadyk, T., Bensmann, B., Krewer, U., and Hanke-Rauschenbach, R., "Modelling and designing cryogenic hydrogen tanks for future aircraft applications," *Energies*, Vol. 11, No. 1, 2018, p. 105. https://doi.org/10.3390/en11010105.

[20] Wilod Versprille, V., "Aerodynamic Shape Optimization of a Liquid-Hydrogen-Powered Blended-Wing-Body," Master's thesis, Delft University of Technology, 2022.

[21] Boeing Commercial Airplanes, "787 Airplane Characteristics for Airport Planning," https://www.boeing.com/resources/boeingdotcom/commercial/airports/acaps/787.pdf, February 2023. Accessed April 20, 2023.

[22] Raymer, D. P., *Aircraft Design: A Conceptual Approach*, 2nd ed., AIAA, 1992.

[23] Brelje, B. J., and Martins, J. R. R. A., "Development of a Conceptual Design Model for Aircraft Electric Propulsion with Efficient Gradients," *Proceedings of the AIAA/IEEE Electric Aircraft Technologies Symposium*, Cincinnati, OH, 2018. https://doi.org/10.2514/6.2018-4979.

[24] Gray, J. S., Hwang, J. T., Martins, J. R. R. A., Moore, K. T., and Naylor, B. A., "OpenMDAO: An open-source framework for multidisciplinary design, analysis, and optimization," *Structural and Multidisciplinary Optimization*, Vol. 59, No. 4, 2019, pp. 1075–1104. https://doi.org/10.1007/s00158-019-02211-z.

[25] Martins, J. R. R. A., and Ning, A., *Engineering Design Optimization*, Cambridge University Press, Cambridge, UK, 2021. https://doi.org/10.1017/9781108980647, URL https://mdobook.github.io.

[26] Wells, D. P., Horvath, B. L., and McCullers, L. A., "The Flight Optimization System Weights Estimation Method," Technical Memorandum TM–2017–219627, NASA, June 2017.

[27] Roskam, J., *Airplane Design Part V: Component Weight Estimation*, DARcorporation, 1989.

[28] Sullivan, R. M., Palko, J. L., Tornabene, R. T., Bednarcyk, B. A., Powers, L. M., Mital, S. K., Smith, L. M., Wang, X.-Y. J., and Hunter, J. E., "Engineering Analysis Studies for Preliminary Design of Lightweight Cryogenic Hydrogen Tanks in UAV Applications," Technical publication NASA/TP–2006-214094, NASA, May 2006. URL https://ntrs.nasa.gov/citations/20060021606.

[29] Budynas, R. G., and Sadegh, A. M., *Roark's Formulas for Stress and Strain, 9th Edition*, McGraw-Hill Education, 2020. Table 15.2.

[30] Jenkinson, L. R., Simpkin, P., and Rhodes, D., *Civil Jet Aircraft Design*, Arnold, 1999.

[31] Jasa, J. P., Chauhan, S. S., Gray, J. S., and Martins, J. R. R. A., "How Certain Physical Considerations Impact Aerostructural Wing Optimization," *AIAA/ISSMO Multidisciplinary Analysis and Optimization Conference*, Dallas, TX, 2019. https://doi.org/10.2514/6.2019-3242.

[32] Jasa, J. P., Hwang, J. T., and Martins, J. R., "Open-source coupled aerostructural optimization using Python," *Structural and Multidisciplinary Optimization*, Vol. 57, No. 4, 2018, pp. 1815–1827.

[33] Chauhan, S. S., and Martins, J. R. R. A., "Low-Fidelity Aerostructural Optimization of Aircraft Wings with a Simplified Wingbox Model Using OpenAeroStruct," *Proceedings of the 6th International Conference on Engineering Optimization, EngOpt 2018*, Springer, Lisbon, Portugal, 2018, pp. 418–431. https://doi.org/10.1007/978-3-319-97773-7_38.

[34] Adler, E. J., and Martins, J. R. R. A., "Efficient Aerostructural Wing Optimization Considering Mission Analysis," *Journal of Aircraft*, 2022. https://doi.org/10.2514/1.c037096.

[35] Torenbeek, E., *Synthesis of Subsonic Airplane Design*, 6$^{\text{th}}$ ed., Delft University Press and Kluwer Academic Publishers, 1990.

[36] Roskam, J., *Airplane Design Part VI: Preliminary Calculation of Aerodynamic, Thrust, and Power Characteristics*, DARcorporation, 1989.

[37] Adler, E. J., Brelje, B. J., and Martins, J. R. R. A., "Thermal Management System Optimization for a Parallel Hybrid Aircraft Considering Mission Fuel Burn," *Aerospace*, Vol. 9, No. 5, 2022. https://doi.org/10.3390/aerospace9050243.

[38] Hendricks, E. S., and Gray, J. S., "pyCycle: A Tool for Efficient Optimization of Gas Turbine Engine Cycles," *Aerospace*, Vol. 6, No. 87, 2019. https://doi.org/10.3390/aerospace6080087.

[39] Maniaci, D. C., "Relative Performance of a Liquid Hydrogen-Fueled Commercial Transport," *46th AIAA Aerospace Sciences Meeting and Exhibit*, 2008. https://doi.org/10.2514/6.2008-152.

[40] Gill, P. E., Murray, W., and Saunders, M. A., "SNOPT: An SQP Algorithm for Large-Scale Constrained Optimization," *SIAM Review*, Vol. 47, No. 1, 2005, pp. 99–131. https://doi.org/10.1137/S0036144504446096.

[41] Wu, N., Kenway, G., Mader, C. A., Jasa, J., and Martins, J. R. R. A., "pyOptSparse: A Python framework for large-scale constrained nonlinear optimization of sparse systems," *Journal of Open Source Software*, Vol. 5, No. 54, 2020, p. 2564. https://doi.org/10.21105/joss.02564.

[42] Bradley, K. R., *A Sizing Methodology for the Conceptual Design of Blended-Wing-Body Transports*, CR-2004-213016, 2004. URL https://ntrs.nasa.gov/citations/20040110949.

[43] Mills, G., "A Comparison of Liquid Hydrogen Tanks for Aircraft," , Aug 2021. Presented at the 2021 AIAA Electric Aircraft Technologies Symposium.

[44] Gardiner, G., "Collins Aerospace to lead COCOLIH2T project," https://www.compositesworld.com/news/collins-aerospace-to-lead-cocolih2t-project-, March 2023. Accessed April 7, 2023.

[45] Kays, C. A., "Multidisciplinary methods for performing trade studies on blended wing body aircraft," Master's thesis, Massachusetts Institute of Technology, 2013. URL https://dspace.mit.edu/handle/1721.1/82485.

[46] Lyu, Z., and Martins, J. R. R. A., "Aerodynamic Design Optimization Studies of a Blended-Wing-Body Aircraft," *Journal of Aircraft*, Vol. 51, No. 5, 2014, pp. 1604–1617. https://doi.org/10.2514/1.C032491.

[47] Yildirim, A., Gray, J. S., and Martins, J. R. R. A., "A Nonlinear Schur Complement Solver for CFD-Based Multidisciplinary Models," *Eleventh International Conference on Computational Fluid Dynamics*, 2022. URL https://www.iccfd.org/iccfd11/assets/pdf/papers/ICCFD11_Paper-0702.pdf, iCCFD11-0702.

[48] Hileman, J. I., Spakovszky, Z. S., Drela, M., Sargeant, M. A., and Jones, A., "Airframe Design for Silent Fuel-Efficient Aircraft," *Journal of Aircraft*, Vol. 47, No. 3, 2010, pp. 956–969. https://doi.org/10.2514/1.46545.